J Mater Sci: Mater Med (2011) 22:29–40
DOI 10.1007/s10856-010-4186-2

Preparation and complex characterization of silica holmium sol–gel monoliths

D. Cacaina · S. Areva · H. Laaksonen · S. Simon · H. Ylänen

Received: 5 January 2010 / Accepted: 9 November 2010 / Published online: 5 December 2010

Abstract Amorphous, sol–gel derived SiO_2 are known to biocompatible and bioresorbable materials. Biodegradable and inert materials containing radioactive isotopes have potential application as delivery vehicles of the beta radiation to the cancer tumors inside the body. Incorporation of holmium in the sol–gel derived SiO_2 could lead to the formation of a biodegradable material which could be used as carrier biomaterial for the radiation of radioactive holmium to the various cancer sites. The homogeneity of the prepared sol–gel silica holmium monoliths was investigated by Back Scattered Electron Imaging of Scanning Electron Microscope equipped with Energy Dispersive X-ray Analysis, X-ray Induced Photoelectron Spectroscopy and Nuclear Magnetic Resonance Spectroscopy. The biodegradation of the monoliths was investigated in Simulated Body Fluid and TRIS (Trizma pre-set Crystals) solution. The results show that by suitable tailoring of the sol–gel processing parameters holmium can be homogeneously incorporated in the silica matrix with a controlled biodegradation rate.

D. Cacaina (✉) · S. Areva · H. Laaksonen · H. Ylänen
Turku Biomaterials Centre, University of Turku, Itäinen Pitkäkatu 4 B (PharmaCity), 20500 Turku, Finland
e-mail: dana.cacaina@yahoo.com

S. Areva · H. Laaksonen · H. Ylänen
Department of Biomedical Engineering, Tampere University of Technology, Biokatu 6, P.O. Box 692, 33101 Tampere, Finland

S. Simon
Faculty of Physics, Babes-Bolyai University, M. Kogalniceanu 1, 400084 Cluj-Napoca, Romania

1 Introduction

The sol–gel technique has been widely used during the last decades as an alternative method for preparing monoliths, fibers, monosized powders and films or coatings of high technology inorganic materials [1–5]. Sol–gel bioceramics such as monoliths, coatings and fibers, are of special interest due to their various medical applications as implants, fillers or drug delivery devices in the human body [6–12].

The sol–gel method allows preparing high purity and homogeneity materials at relative low temperatures with a controlled rate of biodegradability. New generation of ceramic materials with great structural properties has emerged with the sol–gel processing due to the possibility of manipulation and control of the nanostructures. The high porosity and surface area associated with the typical structure of xerogel produced by sol–gel allow obtaining materials with different degradation rate. The possibility of obtaining non-crystalline materials with controlled composition and structures make the sol–gel processing a potential technique for the encapsulation of isotopes for therapeutic applications [12–16].

Biodegradable and non-biodegradable materials containing radioisotopes have been widely investigated as a carrier material for the radiation inside the cancer tumours, in order to provide a high and localized dose of beta radiation [17–28]. Internal radiotherapy using microspheres containing beta radioisotopes represents an alternative for cancer treatment, especially for the cancers where the response to chemotherapy and external radiotherapy is poor. Since the tumors are irradiated in situ the high localized beta radiation replaces the more penetrating external gamma radiation. The choice of beta radioisotope depends on many factors such as: type of the cancer, place

where the cancer is located and the size of the tumor. When choosing the radionuclide the most important parameters which have to be taken into account are the half-life time of the radionuclide, the energy of the beta and gamma radiation if the radioisotope emits both beta and gamma radiation and the range of the radiation in tissues. A short range irradiation reduces the risk of damage to healthy tissue and also provides the possibility for a high radiation dose in a short period of time [13, 29–34].

Internal radiotherapy using non-biodegradable microspheres are currently used in the treatment of liver cancer [35, 36]. Both biodegradable and inert microspheres have been widely investigated for treatment of different kind of cancers like liver, brain and bone cancer and rheumatoid arthritis [17, 18, 24–30, 35, 36]. Non-biodegradable microspheres remain as impurities in the target area after the radioactivity decays. However, dissolution and elimination of the particles from the body after their deactivation would be desirable [29–34].

The present work proposes the development of biodegradable sol–gel derived SiO_2 xerogels containing holmium as potential biomaterial to be used as matrix material for carrying of the radioactive holmium to the cancer sites inside the body. The beta radiation of holmium has suitable characteristics for radiotherapy [22–30]. The silica holmium radioactive particles could locally deliver high dose of beta radiation for killing the cancerous cells and biodegrade after the release of radiation.

The homogeneity of the monoliths was analysed by means of Back Scattered Electron Imaging of Scanning Electron Microscopy equipped with Energy Dispersive X-ray Analysis (BEI-SEM/EDX) and X-ray Photoelectron Spectroscopy (XPS). Characterization of the materials was done by N_2 sorption isoterms and Nuclear Magnetic Resonance Spectroscopy (NMR). The in vitro degradation of the monoliths was investigated in TRIS buffered solution (Trizma pre-set Crystals, Sigma) and Simulated Body Fluid (SBF) by analyzing the concentration of silica, calcium and phosphorous in the immersion solutions, using UV–VIS Spectroscopy.

2 Materials and methods

2.1 Materials preparation

The holmium silica monoliths were prepared by the hydrolysis and polycondensation of tetraethoxysilane (TEOS 98%, Aldrich). Holmium(III) nitrate pentahydrate 99.9% ($Ho(NO_3)_3{\cdot}5H_2O$) was used as precursor for holmium in the monoliths. The nitrate powder was added to the hydrolysed sol. Nitric acid (HNO_3) was used as a catalyst and both nitric acid and ammonium hydroxide (NH_4OH) were used for adjusting the pH. Different H_2O/TEOS mole ratios (R), pH and concentration of holmium, were used for the preparation of the sols. The silica sol–gel process is strongly dependent on the water-to-silica precursor ratio, pH and temperature [15, 37].

Two groups of monoliths (groups A and B) were prepared in order to optimize the preparation parameters and procedure. Both groups contain 10% Ho_2O_3, with the R (H_2O/TEOS ratio) of 5, 15, 20, 25 and 30, and the pH of 1 and 2.

The monoliths were prepared in a cylindrical polystyrene moulds (8 × 13 mm). The sol was injected into the moulds where the gelation and drying occurred. The drying stage is very important if homogeneous, crack-free materials are desired. Especially for monoliths the drying has to be slow in order to avoid cracking. The aging and drying of the monoliths have been done in two different environments, at room temperature, RT (group A) and in the controlled environment CE, at 40°C and 40% relative humidity (group B). The goal of using different aging and drying procedure is to optimize the preparation procedure in order to obtain homogeneous monoliths without holmium separation into the silica network. The aging time of the sol was between 24 and 48 h, in both conditions. The formed gel of the samples from group B was slowly dried for 48 h at 40°C and 40% relative humidity, and then fast dried for 24 h in the same environment. The samples aged at room temperature, group A, were slowly dried 48 h at room temperature and then fast dried for 24 h at 40°C and 40% relative humidity. The drying process at 40°C is a slow and unforced process done at constant conditions, where the gel structure is formed. The sol–gel formulation for the monoliths prepared at the two environments is given in Table 1.

After drying, the monoliths were thermally treated in two different ways, fast and slow, at different temperatures.

Table 1 The sol–gel formulation for the monoliths prepared in the two environments (RT and CE)

Monoliths A prepared at RT	Monoliths B prepared at CE	R (H_2O/TEOS ratio)	pH
A01	B01	15	1
A02	B02	15	2
A11	B11	20	1
A12	B12	20	2
A21	B21	25	1
A22	B22	25	2
A41	B41	30	1
A42	B42	30	2
A51	B51	5	1
A52	B52	5	2

Different thermal treatment procedure, treatment temperatures and treatment time, was applied with the aim to optimize both the biodegradation rate and the homogeneity of the monoliths. The fast thermal treatment was applied with a heating rate of 100°C/h at 300, 500 and 700°C. The treatment time was 30 min and 2 h, and then the samples were cooled down with the oven at room temperature. The slow thermal treatment was applied with a heating rate of 10°C/h up to 300°C, kept there for 2 h and then the temperature increases to the desired values (500 and 700°C) with an increasing rate of 60°C/h. The treatment time was 2 h at 500 and 700°C and then the samples were cooled down with the oven at room temperature. The complex characterization of the monoliths allowed us to select the preparation procedure and parameters. Thus, the controlled environment was selected as the preparation procedure and the following parameters were used for the preparation of the final monoliths: R = 30, pH 2, and the thermal treatment temperature of 500 and 700°C.

The selected procedure and parameters were then applied for the preparation of monoliths with different holmium concentration, silica monoliths with 1% Ho_2O_3 (group D) and silica monoliths with 5% Ho_2O_3 (group C).

2.2 Materials characterization

The distribution of holmium in the prepared monoliths was analysed by means of Back Scattered Electron Imaging of Scanning Electron Microscopy (BEI-SEM). The concentration of holmium in several random selected positions on the cross section of the monolith was measured by Energy Dispersive X-Ray analysis. Monolith samples embedded in acrylic resin was used for the measurements. After hardening of the resin, the samples were polished and the polished surface was coated with a thin layer of carbon.

The pore structure of the prepared monoliths was also investigated. The Brunauer, Emmet and Teller (BET) method was used to calculate the specific surface area from the (N_2) adsorption and desorption isotherms.

X-ray induced photoelectron spectroscopy offers information on the first 50-100 Å of the sample surface and it is a key tool in understanding the chemistry and physics taking place on surfaces and at interfaces, that is, in particular, of special interest for biomaterials.

X-ray Photoelectron Spectroscopy (XPS) analyses were performed on SPECS PHOIBOS 150 MCD system with monochromatised Al Kα radiation from a 300 W X-ray source ($h\nu = 1486.6$ eV). The measurements were carried out under ultra high vacuum conditions, of order 10^{-10} Torr. A low energy electron beam was used to achieve charge neutrality at the sample surface. The binding energy scale was calibrated using the C 1s line at 284.6 eV.

^{29}Si MAS-NMR spectra were recorded on MAS-NMR AVANCE 400 Bruker spectrometer, at 79.5 MHz, in a 9.4 T field, with a rotation frequency of samples at magic angle spinning of 6 kHz (for samples containing 1% Ho_2O_3) and 10 kHz (for samples containing 10% Ho_2O_3). The reference for the chemical shift (0 ppm) was tetramethylsilane (TMS). Due to the high concentration of paramagnetic holmium ions, Ho^{3+}, the intensity of the samples with 10% Ho_2O_3 was quite low. For these samples the number of scans was almost three times the number of scans for samples with 1% Ho_2O_3.

2.3 Materials biodegradation

The silica holmium particles with a diameter of 315–500 μm were obtained by crushing and sieving the prepared monoliths. The obtained particles were immersed in 0.05 M TRIS (Trizma pre-set Crystals, Sigma) solution buffered at pH 7.4, T = 37°C, for 7 days. For the first immersion days the SiO_2 in TRIS was kept below 30 ppm (to ensure sink conditions; free dissolution of SiO_2 matrix). The saturation level at pH 7.4 is about 130 ppm. The biodegradation tests were done also in Simulated Body Fluid (SBF) solution with a pH at 7.4, T = 37°C for up to 14 days.

The silica concentration in both immersion solutions was measured with UV–VIS spectrophotometer (UV-1601, Shimadzu) analysing the molybdenum blue complex absorbance at 820 nm. The calcium and phosphorus in the SBF solution was also measured using the same UV–VIS spectrophotometer.

3 Results and discussion

3.1 Materials characterization

BEI-SEM/EDX analysis results show the distribution of holmium in the monolith and the homogeneity of the monolith. For the intended application the homogeneity of the material is a very important parameter in order to achieve a local homogeneous dose of radiation in the target site.

Moreover, the results indicate that the parameters used for preparation and thermal treatment of the monoliths influence the distribution of holmium in the silica network of the monolith.

Figures 1 and 2 show the SEM images of the prepared monolith with 10% Ho_2O_3, R = 30, pH 2 (B42) before and after thermal treatment at 700°C for 2 h. Table 2 shows the concentration of SiO_2 and Ho_2O_3 as measured by EDX.

As can be seen from the Fig. 1, in the as-prepared monolith holmium is not homogeneously distributed in the

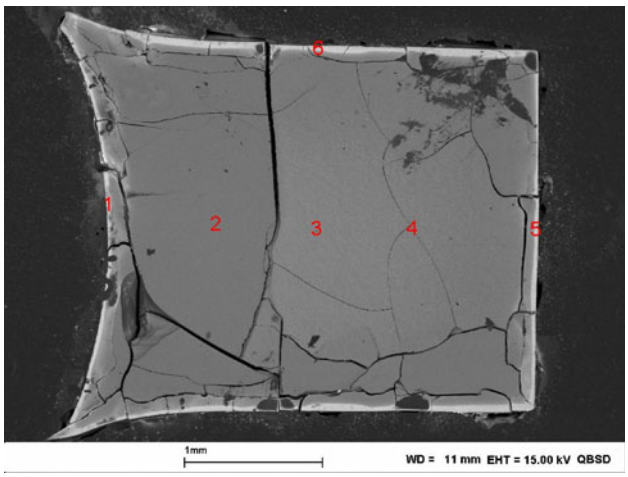

Fig. 1 SEM image of the B42 monolith, 10% Ho_2O_3, R = 30, pH 2, as-prepared

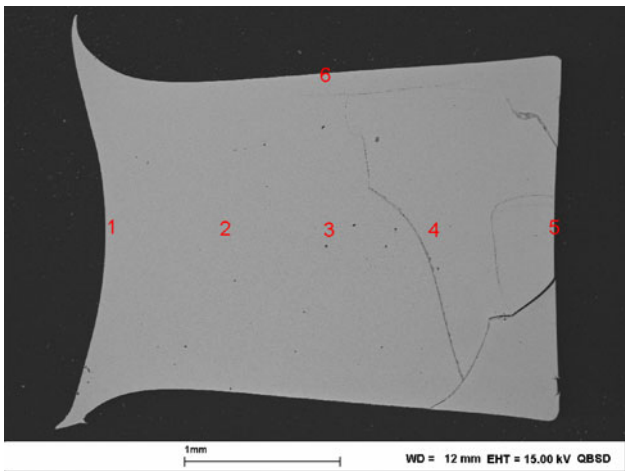

Fig. 2 SEM image of the B42 monolith, 10% Ho_2O_3, R = 30, pH 2, thermally treated at 700°C/2 h

silica network. A high concentration of holmium is present on the surface of the monolith as can be seen in the SEM image (the white part on the surface of the monolith). The concentration of holmium was measured in several random selected positions in the cross section of the as-prepared monolith by EDX analysis and the results are given in Table 2. After thermal treatment, holmium is quite homogeneously distributed in the silica network of the monolith as can be observed in Fig. 2. It can be concluded that the homogeneity of the monolith is obtained only after thermal treatment and is not influenced by the parameters used in sol–gel formulation, aging and drying of the monoliths. The concentration of holmium in different positions in the cross section of the thermal treated monolith measured by EDX analysis is shown in Table 2. In the present study, the prepared monoliths were thermally treated at three different temperatures: 300, 500 and 700°C, for 30 min and 2 h, in order to point out the influence of the treatment temperature and treatment time on the distribution of holmium in the monolith during the treatment procedure. A fast and slow thermal treatment was also applied to investigate whether this would affect the homogeneity of the monolith. The SEM investigations on those monoliths showed that the treatment temperatures used does not influence the homogeneity of the monolith, since homogeneous monoliths can be obtained at the treatment temperature as low as 300°C and as high as 700°C. Homogeneous distribution of holmium in the monoliths can be observed at both, 30 min and 2 h thermal treatment time. Also, the fast and slow thermal treatment procedure does not influence the homogeneity of the monoliths for the selected treatment temperatures and treatment time.

Sol–gel produced materials are typically nanoporous in nature. N_2 sorption was used to measure the specific surface area according to the method of Brunauer, Emmett and Teller, so called BET surface area. The N_2 adsorption–desorption isotherms for the two monoliths with 1% Ho_2O_3 (D42) and 10% Ho_2O_3 (B42) thermally treated at 300 and 700°C for 2 h, are shown in the Figs. 3 and 4. The BET surface area and the pore analysis results are presented in Table 3.

The pore structure analysis gives valuable information about the formation of the structure and its influence on the

Table 2 Concentration of SiO_2 and Ho_2O_3 (wt%) as measured by EDX

B42-10% Ho_2O_3, R = 30, pH 2, as-prepared			B42-10% Ho_2O_3, R = 30, pH 2, thermal treated at 700°C/2 h		
Position	SiO_2 (wt%)	Ho_2O_3 (wt%)	Position	SiO_2 (wt%)	Ho_2O_3 (wt%)
Spot 1	73.24	26.76	Spot 1	86.06	13.94
Spot 2	94.49	5.51	Spot 2	89.33	10.67
Spot 3	94.57	5.43	Spot 3	90.58	9.42
Spot 4	92.34	7.66	Spot 4	88.79	11.21
Spot 5	76.48	23.52	Spot 5	86.55	13.45
Spot 6	77.42	22.58	Spot 6	84.21	15.79

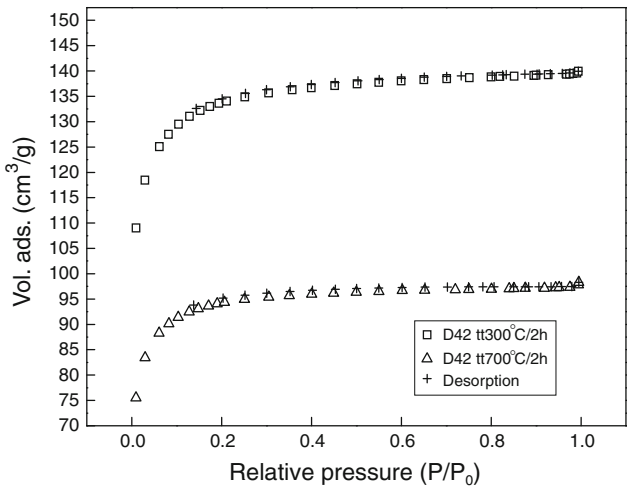

Fig. 3 N_2 adsorption–desorption isotherms for the monoliths D42 thermally treated at 300 and 700°C for 2 h

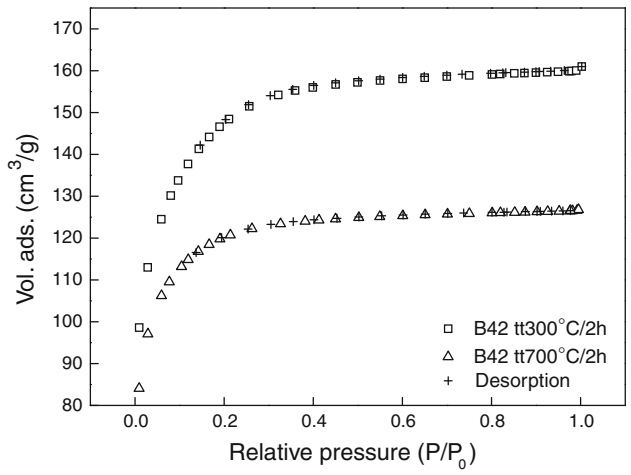

Fig. 4 N_2 adsorption–desorption isotherms for the monoliths B42 thermally treated at 300 and 700°C for 2 h

bioactivity and biodegradability of the monoliths. High BET surface area is related to a high porosity. As can be observed from the Table 3, when the holmium concentration increases the BET-surface area also increases. The increase of the treatment temperature induced the decreasing of the BET-surface area. The studied samples contain mostly micropores, although with slight mesoporosity (porosity of diameter 2-50 nm). The mesopore volume decreases by increasing of the holmium concentration and the treatment temperature. However, for the samples thermally treated at 700°C there is no difference between the mesopore volumes, even if the concentration of holmium is different. Also, there is a small difference in the mesopore volume for the sample with 10% Ho_2O_3 thermally treated at the two temperatures compared with the samples with 1% Ho_2O_3. The micropore volume increases by increasing of the holmium concentration and decreases by increasing of the treatment temperature. The diameter of the pores increases by increasing the concentration of holmium, and decreases by increasing the treatment temperature for the samples with 10% Ho_2O_3 while for the samples with 1% Ho_2O_3, a very small difference in the diameters of the pores is observed by increasing the treatment temperature.

The results indicate that silica alone mainly determines the porous structure of the monolith. The holmium species likely only fill the pores, which are formed when the silica species aggregate.

Holmium introduced as dopand in the materials also affects the mechanical strength of the monoliths. Increased concentration of holmium produces more crystallinity causing extra stresses.

The composition and structure together determine the in vitro bioactivity of the sol–gel monoliths. In pure silica, the great mesopore volume and the wide distribution of the mesopores favor the hydroxyapatite nucleation, while the surface area does not influence so much the bioactivity of the materials [38].

The XPS survey spectra of the B42 (10% Ho_2O_3) and D42 (1% Ho_2O_3) samples thermally treated at 500 and 700°C are given in Fig. 5. The XPS results indicate that the samples are of high purity. From the spectra it can be seen a low carbon peak, but carbon adsorption occurs on all surfaces exposed to the atmosphere and is detected by the XPS technique [39, 40]. Actually, the binding energy (BE) of this peak was considered for the calibration of the photoelectron spectra. The position and full width at half maximum (FWHM) of photoelectron peaks were estimated using spectra simulation based on summation of Lorentzian and Gaussian functions.

The elemental composition of the samples was determined in at.% from the survey spectra (Fig. 5). The results

Table 3 Summary of sorptometer results

Sample code	Treatment temp. (°C)	BET surface area (m^2/g)	$V_{Micropore}$ (cm^3/g)	$V_{Mesopore}$ (cm^3/g)	$V_{Total\ pore}$ (cm^3/g)	Pore width (Å)
B42	300	538.6	0.2341	0.0119	0.2460	25.83
B42	700	449.3	0.1833	0.0113	0.1946	16.31
D42	300	510.1	0.1956	0.0191	0.2147	15.64
D42	700	361	0.1392	0.0112	0.1504	16.31

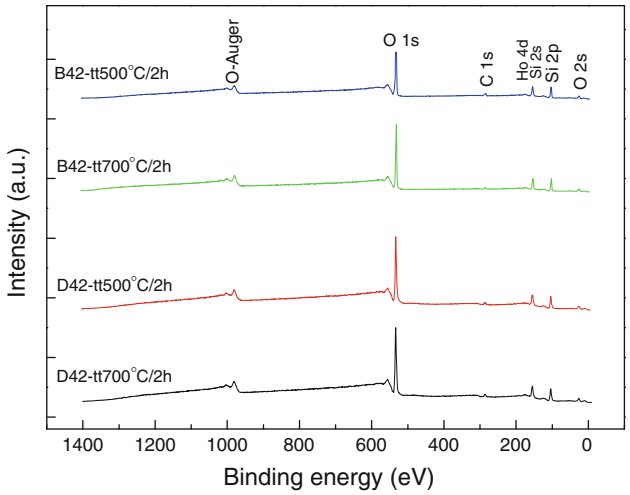

Fig. 5 Survey spectra of the B42 and D42 monoliths thermal treated at 500 and 700°C for 2 h

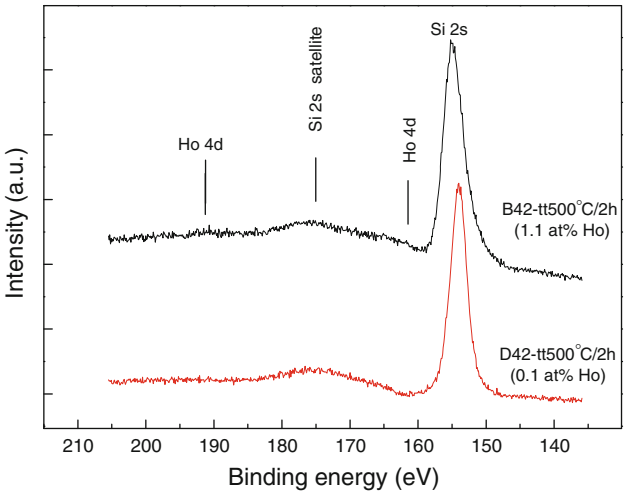

Fig. 6 XPS spectra of the B42 and D42 monoliths thermal treated at 500°C for 2 h recorded in the binding energy range corresponding to 4d Ho and 2s Si X-ray photoelectrons

are summarized in Table 4. For comparison are also included the expected values, as they were considered for the samples preparation.

The high resolution spectrum of Ho 4d photoelectrons is scarcely recordable even for B42 samples, due to their low holmium content (circa 1 at.%). However, for the 1 at.% holmium containing samples (B42), different from those with 0.1 at.% holmium (D42), the smoothed core-level spectrum (Fig. 6) evidences the features of X-ray photoelectron 4d core-level multiplets for holmium [41] overlapped by the satellite of Si 2s photoelectron peak, occurring due to inelastic scattering of the electrons.

The O 1s, Si 2p and Si 2s core level photoelectron spectra of the samples B42 and D42 thermally treated at 700°C for 2 h are given in Figs. 7, 8, 9. The photopeaks of D42 samples are rather symmetric and can be well fitted to a single peak, while that recorded from B42 samples are less symmetric and better fitted with two components.

By rising the heat treatment temperature from 500 to 700°C, for B42 sample one remarks an decrease of BE and an increase of FWHM values, while for D42, with very low holmium content, these values seem to be practically unaffected, but in fact both BE and FWHM increase (Table 5).

The line broadening for these monoliths with very high silica content indicates that 700°C heat treatment enhances the vitreous state stability. By inspecting the samples heat treated at 700°C one observes a decrease in binding energy of silicon core level electrons as 10 wt% Ho_2O_3 is added to the silicate glass matrix that denotes an increase in electron density around the Si atoms. An opposite effect is observed for the 500°C heat treated samples. This is correlated with fact that the effective electronic charge density on a cation decreases as the number of oxygen anions increases. The decrease in effective electronic charge density around the cations would be reflected in an increase in the binding energy of the remaining electrons [42, 43].

The ^{29}Si MAS-NMR spectra of 1% Ho_2O_3 and 10% Ho_2O_3 samples (Fig. 10) show larges widths for the lines recorded from the samples with 10% Ho_2O_3, due to the disordering effect of holmium on SiO_2 vitreous matrix. The structure of the silicate network in glass systems is mainly determined by the degree of polymerization of the silicate tetrahedra and described by the abundance of different Q^n species, where Q^n denotes a tetrahedron linked by bridging O atoms to n adjacent tetrahedra. The range of n is 0, for isolated tetrahedra, to 4, for fully polymerized three-dimensional network [44].

Table 4 Atomic percentage of the elements obtained from XPS analysis

Sample code	Treatment temp. (°C)	Ho (at.%)		Si (at.%)		O (at.%)	
		Expected	Measured	Expected	Measured	Expected	Measured
B42	500	1.14	1	32.38	30.3	66.48	68.7
B42	700		0.9		31.2		67.9
D42	500	0.11	–	33.24	30.1	66.65	69.9
D42	500		–		31.5		68.5

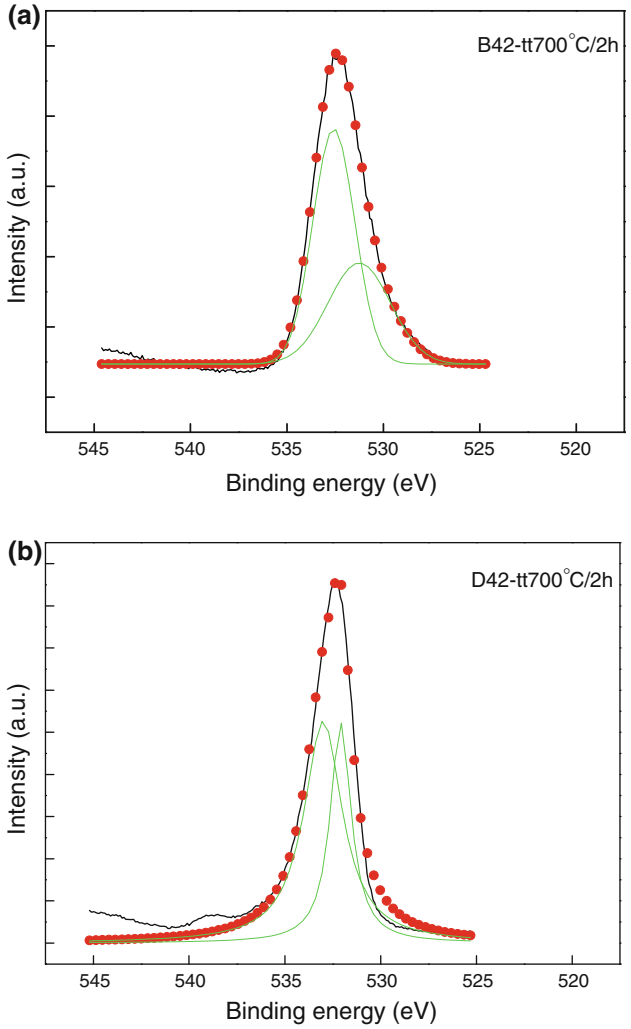

Fig. 7 O 1s core level photoelectron spectra of the B42 (**a**) and D42 (**b**) monoliths thermal treated at 700°C for 2 h

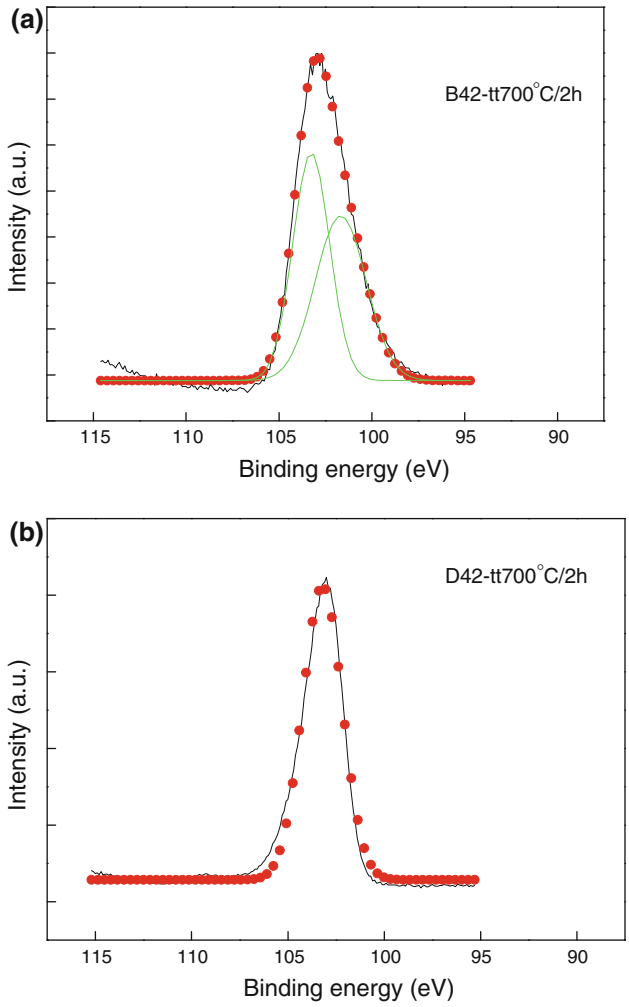

Fig. 8 Si 2p core level photoelectron spectra of the B42 (**a**) and D42 (**b**) monoliths thermal treated at 700°C for 2 h

According to chemical shift values of component lines obtained from spectra deconvolution by DMfit program [45] (Table 6) the structural units are mainly Q^4 species, but also Q^3 species are evidenced, as can be seen from Fig. 11 for the sample with 1% Ho_2O_3 heat treated at 500°C for 2 h.

The chemical shift in the ^{29}Si MAS NMR spectra depends on heat treatment temperature reflecting differences in the local order of the silicate network, expected for different processing conditions of the samples [45]. By increasing the heat treatment temperature, the fraction of Q^4 species and the corresponding line-width increase, showing a higher degree of network polymerisation and a larger local disorder, particularly in samples with 10% Ho_2O_3. The occurrence of Q^n-species with prevalent high n values is consistent with ^{29}Si MAS NMR results reported for sol–gel derived silicate systems [46, 47].

3.2 Materials biodegradation

The SiO_2 dissolution of sol–gel produced silica matrices depends upon porosity and the chemical structure. Sol–gel produced materials are typically porous by nature, but the porosity and the chemical structure depends on the used preparation parameters, such as precursors and their concentration, preparation method and temperature. The dissolution of the sol–gel produced silica holmium monoliths was measured in pH buffered TRIS solution and in SBF solution with a pH at 7.4, at T = 37°C.

The silica release behavior in the TRIS solution for the samples with 10% Ho_2O_3, thermally treated at 500°C for 2 h with R = 5 (B52), R = 15 (B02), R = 30 (B42) is shown in Fig. 12. As can be seen from the figure, the increase of R induces the increase of the silica release in the solution. About 20% of silica was released into the solution during the immersion time from the sample with

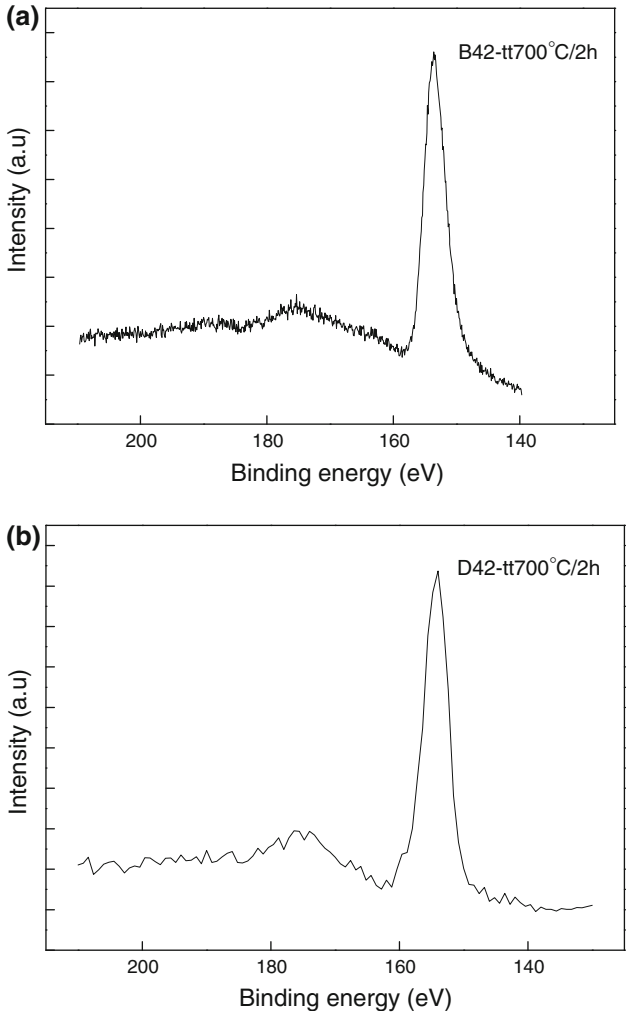

Fig. 9 Si 2s core level photoelectron spectra of the B42 (**a**) and D42 (**b**) monoliths thermal treated at 700°C for 2 h

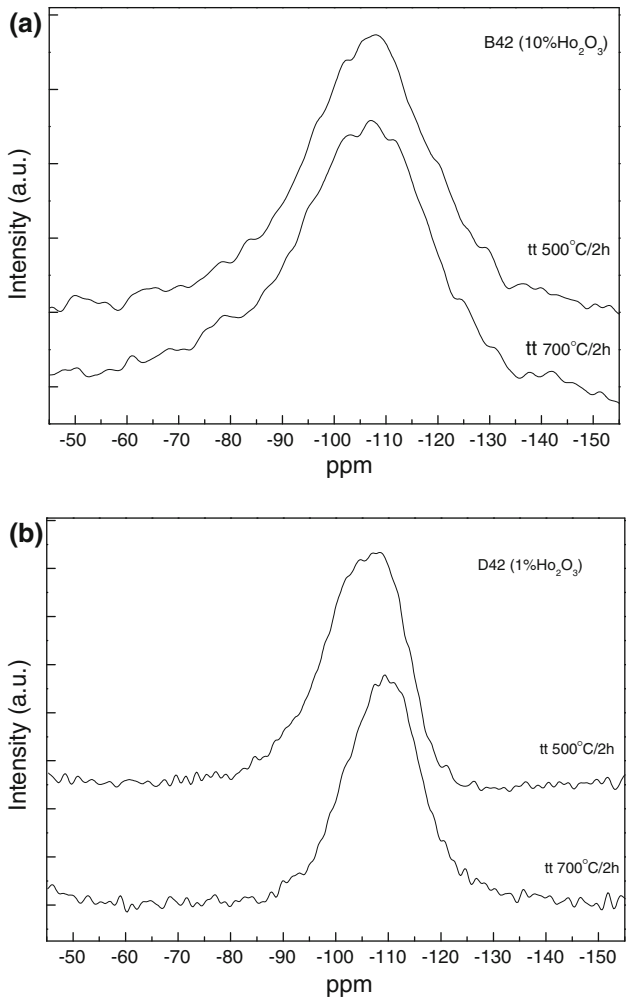

Fig. 10 NMR spectra of the B42 (**a**) and D42 (**b**) monoliths thermally treated at 500 and 700°C for 2 h

R = 30 (B42), while for the sample with R = 5 (B52) only about 1.5% of silica was released.

Figures 13 and 14 show the biodegradation results for the samples with different holmium content, 10% Ho_2O_3 (B42), 5% Ho_2O_3 (C42) and 1% Ho_2O_3 (D42), with R = 30, pH 2, thermally treated at 500 and 700°C for 2 h. The decrease of the concentration of holmium oxide induces a decrease of the biodegradation rate. The higher release of silica from the B42 sample compared with the other two samples could be due to the more porous structure and higher surface area as the N_2-sorption results indicate. The results show that the increase of the thermal treatment temperature induces a slower release of silica into the TRIS solution during the immersion time.

The SiO_2 matrix degradation is influenced by the water/TEOS ratio, concentration of holmium and thermal treatment temperature. The rate of degradation can be easily controlled by suitable tailoring of those parameters.

The degradation of the monoliths occurs also in the SBF solution. The B42, C42 and D42 samples thermally treated

Table 5 Core level electron binding energies (BE) and full-width at half-maximum (FWHM)

Sample code	Treatment temp. (°C)	O 1s		Si 2p		Si 2s	
		BE (eV)	FWHM (eV)	BE (eV)	FWHM (eV)	BE (eV)	FWHM (eV)
B42	500	533.20	2.60	103.93	2.46	154.79	2.81
	700	532.25	2.66	102.64	2.80	153.45	3.07
D42	500	532.39	2.00	103.03	1.98	154.03	2.39
	700	532.53	2.11	103.21	2.06	154.33	3.27

Table 6 Chemical shift, δ, full width at half maximum of component lines obtained by ^{29}Si MAS NMR spectra deconvolution, and the distribution of $Q^{(n)}$ units

Sample code	Treatment temp. (°C)	Q^n	Line position, δ (ppm)	Line width (ppm)	Q^n population (%)
B42	500	Q^4	−106.5	15.0	89.1
		Q^3	−92.0	12.1	10.9
	700	Q^4	−109.3	16.4	95.8
		Q^3	−96.5	7.6	4.2
D42	500	Q^4	−108.9	16.4	84.3
		Q^3	−95.00	13.1	15.7
	700	Q^4	−109.8	25	92.3
		Q^3	−93.4	12.5	7.7

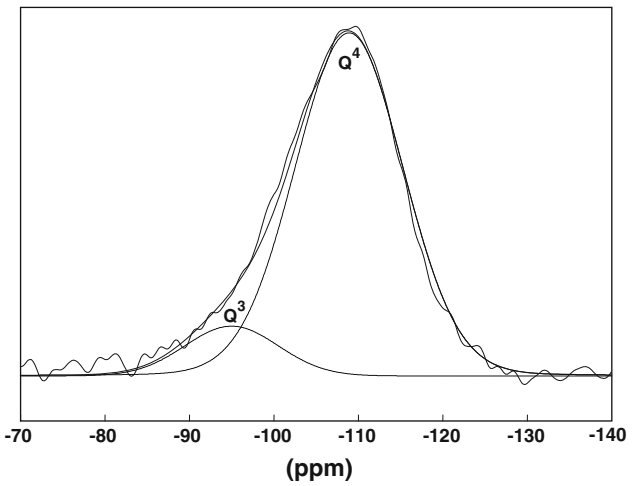

Fig. 11 ^{29}Si MAS NMR experimental and simulated spectra along with the deconvolution components, for D42 monolith thermally treated at 500°C for 2 h

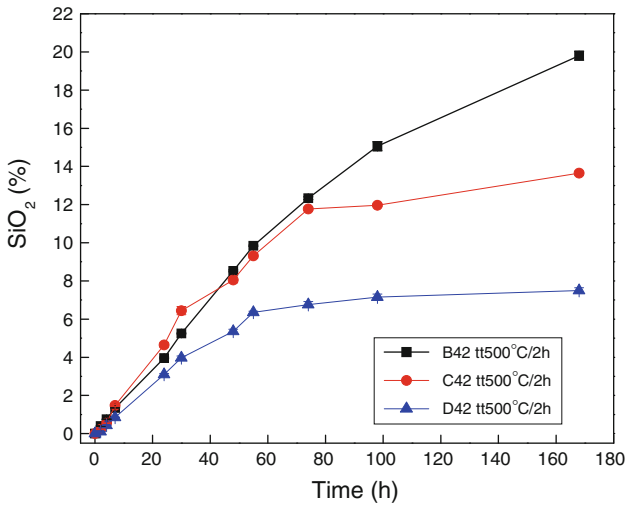

Fig. 13 Silica release in the immersion TRIS solution for the B42 (10% Ho_2O_3), C42 (5% Ho_2O_3) and D42 (1% Ho_2O_3) monoliths with R = 30, pH 2, thermally treated at 500°C for 2 h

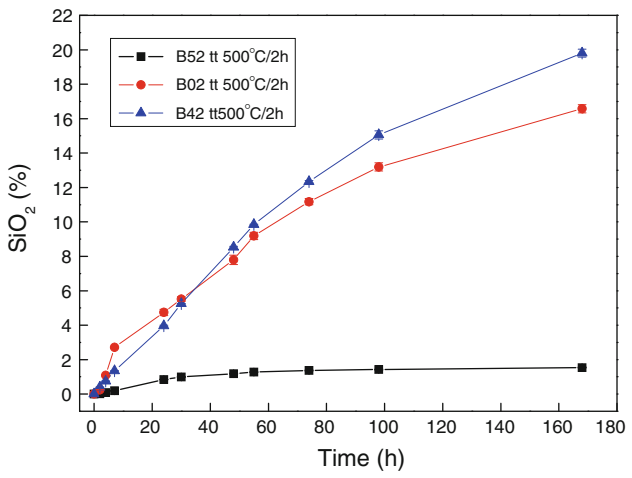

Fig. 12 Silica release in the immersion TRIS solution for the monoliths with 10% Ho_2O_3 and R = 5 (B52), 15 (B02) and 30 (B42), pH 2, thermally treated at 500°C for 2 h

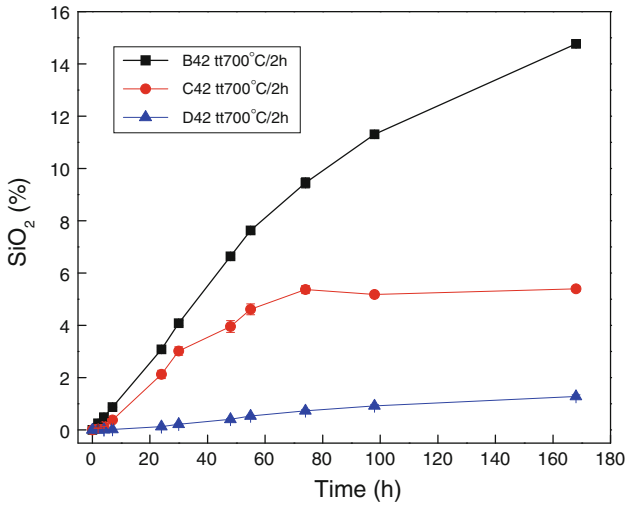

Fig. 14 Silica release in the immersion TRIS solution for the B42 (10% Ho_2O_3), C42 (5% Ho_2O_3) and D42 (1% Ho_2O_3) monoliths with R = 30, pH 2, thermally treated at 700°C for 2 h

at 500°C for 2 h were immersed in SBF solution for up to 14 days. The concentration of P, Ca and Si in the SBF solution after the immersion time was analyzed by UV–VIS spectroscopy and the results are presented in Figs. 15, 16, and 17.

As can be seen from the Fig. 17, silica is released in the immersion solution showing the degradation of the silica matrix of the monoliths in SBF solution. Calcium and phosphorous concentration decreases after the immersion in SBF indicating a precipitation of calcium and phosphate species from the solution on the monoliths surface (Figs. 15, 16).

In order to point out the calcium phosphate precipitate on the surface of the monoliths the immersed monoliths were analysed by SEM–EDX. Figures 18 and 19 show the calcium phosphate precipitates formed on the particles surface (D42 and B42 monoliths, thermally treated at 500°C for 2 h) during the immersion for 7 days in SBF. The particles with 1% Ho_2O_3 (D42) thermally treated at 500°C for 2 h exhibits calcium phosphate precipitate on their surface after immersion in SBF (Fig. 18) while a thick reaction calcium phosphate layer rich in holmium was formed on the particles surface with 10% Ho_2O_3 (B42) thermally treated at 500°C for 2 h, during the immersion in

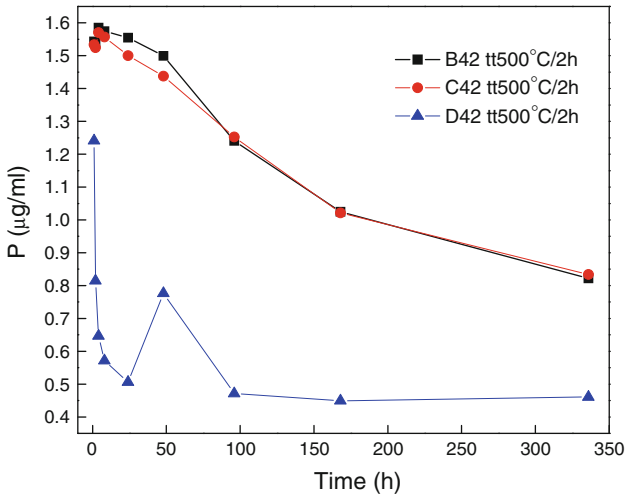

Fig. 15 Phosphorous concentration in the immersion SBF solution for the B42 (10% Ho_2O_3), C42 (5% Ho_2O_3) and D42 (1% Ho_2O_3) monoliths with R = 30, pH 2, thermally treated at 500°C for 2 h

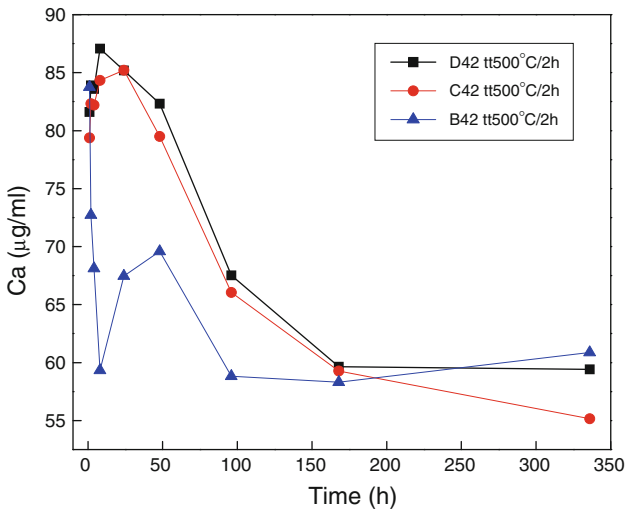

Fig. 16 Calcium concentration in the immersion SBF solution for the B42 (10% Ho_2O_3), C42 (5% Ho_2O_3) and D42 (1% Ho_2O_3) monoliths with R = 30, pH 2, thermally treated at 500°C for 2 h

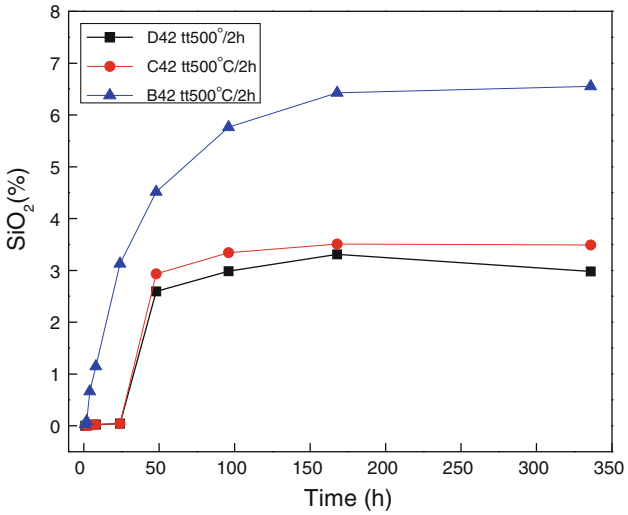

Fig. 17 Silica release in the immersion SBF solution for the B42 (10% Ho_2O_3), C42 (5% Ho_2O_3) and D42 (1% Ho_2O_3) monoliths with R = 30, pH 2, thermally treated at 500°C for 2 h

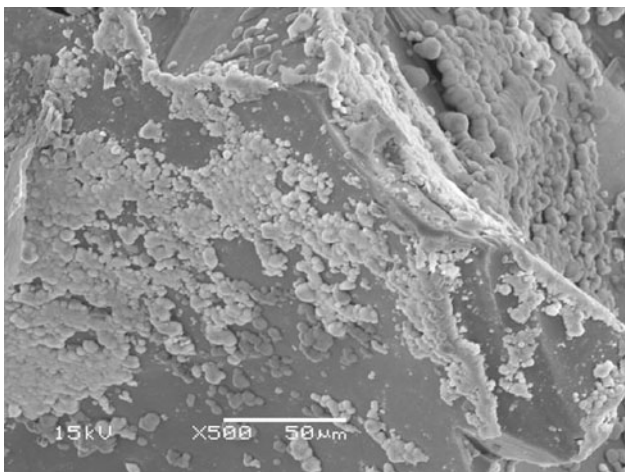

Fig. 18 SEM image of the D42 (1% Ho_2O_3) monolith with R = 30, pH 2, thermally treated at 500°C for 2 h after 7 days immersion in SBF

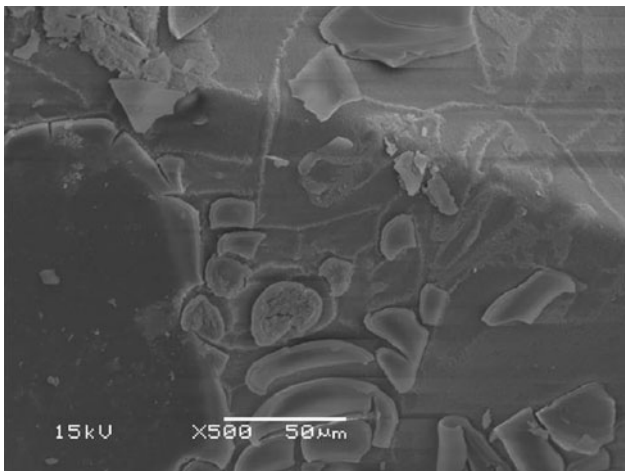

Fig. 19 SEM image of the B42 (10% Ho_2O_3) monolith with R = 30, pH 2, thermally treated at 500°C for 2 h after 7 days immersion in SBF

SBF (Fig. 19). The SEM results are well correlated with the biodegradation results.

The decrease in the calcium and/or phosphate concentration is accepted to an indication of the HCA formation leading possible to the bioactivity.

4 Conclusions

The results show that promising biomaterials able to carry the radioactive holmium, the source of beta radiation, in the body can be produced by sol–gel method. Structural characterization of the materials indicates that homogenous and crack-free silica monoliths incorporated holmium can be obtain when a suitable sol–gel processing and thermal treatment are applied. The properties of the materials are determined by both the structure and composition. The thermal treatment applied influences also the degradation of the materials in TRIS and SBF solutions. The biodegradation results indicate that biodegradable materials with controlled biodegradation rate could be obtain by suitable tailoring of the composition, structure and thermal treatment. Calcium phosphate precipitates are formed on the particle surface, when immersed in the SBF solution. Holmium in the monoliths seems to favor the calcium phosphate precipitates since a thick calcium phosphate layer is formed on the particles with the highest amount of holmium (10% Ho_2O_3). The behavior of the prepared silica holmium monoliths in the tested environments are influenced by the composition of the materials and the thermal treatment applied.

Acknowledgments The Finnish Funding Agency for Technology and Innovation (TEKES—Project 40118/06) is acknowledged for the financial support of this work. Thanks to T. Radu and R.V.F. Turcu from Babes-Bolyai University for the XPS and NMR measurements and Department of Physical Chemistry of Åbo Akademi University for N_2-sorption measurements.

References

1. Hench LL, Wilson J. Introduction to bioceramics. In: Hench LL, Wilson J, editors. Introduction to bioceramics, vol. 1. Singapore: World Scientific; 1993. p. 1–24.
2. Livage J, Henry M, Sanchez C. Sol–gel chemistry of transition metal oxides. Prog Solid State Chem. 1988;18:259–341.
3. Kepinski L, Wolcyrz M. Nanocrystalline rare earth silicates: structure and properties. Mater Chem Phys. 2003;81:396–400.
4. Aparicio M, Duran A. Preparation and characterization of $50SiO_2$–$50Y_2O_3$ sol–gel coatings on glass and SiC(C/SiC) composites. Ceram Int. 2005;31:631–4.
5. Parmentier J, Liddell K, Thompson DP, Lemercier H, Schneider N, Hampshire S, Bodart PR, Harris RK. Influence of iron on the synthesis and stability of yttrium silicate apatite. Solid State Sci. 2001;3:495–502.
6. Jokinen M, Rahiala H, Rosenholm JB, Peltola T, Kangasniemi I. Relation between aggregation and heterogeneity of obtained structure in sol–gel derived CaO–P_2O_5–SiO_2. J. Sol–Gel Sci Technol. 1998;12:159–67.
7. Viitala R, Jokinen M, Peltola T, Gunnelius K, Rosenholm JB. Surface properties of in vitro bioactive and non-bioactive sol–gel derived materials. Biomaterials. 2002;23:3073–86.
8. Yoshida K, Tanagawa M, Kamada K, Hatada R, Bada K, Inoi T, Atsuna M. Silica coatings formed on noble dental casting alloy by the sol–gel dipping process. J Biomed Mater Res. 1999;46:221–7.
9. Pereira M, Clark AE, Hench LL. Effect of texture on the rate of hydroxyapatite formation on gel–silica surface. J Am Ceram Soc. 1995;78:2463–8.
10. Sepulveda P, Jones JR, Hench LL. Characterization of melt-derived 45S5 and sol–gel-derived 58S bioactive glasses. J Biomed Mater Res (Appl Biomater). 2001;58:734–40.
11. Zhong J, Greenspan DC. Processing and properties of sol–gel bioactive glasses. J Biomed Mater Res (Appl Biomater). 2000;53:694–701.
12. Ramila A, Vallet-Regi M. Static and dynamic in vitro study of a sol–gel glass bioactivity. Biomaterials. 2001;22:2301–6.
13. Roberto WS, Pereira MM, Campos TPR. Structure and dosimetric analysis of biodegradable glasses for prostate cancer treatment. Artif Organs. 2003;27(5):420–4.
14. Cacaina D, Viitala R, Jokinen M, Ylänen H, Hupa M, Simon S. In vitro behavior of yttrium silica sol–gel microspheres. Key Eng Mater. 2005;411:284–6.
15. Brinker CJ, Scherer GW. Sol–gel science: the physics and chemistry of sol–gel processing. New York: Academic Press; 1990.
16. Cacaina D, Turcu RVF, Udvar DA, Vaahtio M, Ylänen H, Simon S. Structural characterization of yttrium silica sol–gel microspheres. J Optoelectron Adv Mater. 2007;9(8):2566–70.
17. White JE, Day DE. Rare earth aluminosilicate glasses for in vivo radiation delivery. Key Eng Mater. 1994;94–95:181–208.
18. Kawashita M, Shineha R, Kim HM, Kokubo T, Inoue Y, Araki N, Nagata Y, Hiraoka M, Sawada Y. Preparation of ceramic microspheres for in situ radiotherapy of deep-seated cancer. Biomaterials. 2003;24:2955–63.
19. Lin W, Tsai S, Hsieh J, Wang S. Effects of ^{90}Y microspheres on liver tumors: Comparison of intratumoral injection method and intra-arterial injection method. J Nucl Med. 2004;41:1892–7.
20. Kennedy A, Coldwell D, Nutting C, Murthy R, Wertman DE, Loehr SP, Overton C, Meranze S, Niedzwiecki J, Sailer S. Resin

^{90}Y-microsphere brachytherapy for unresectable colorectal liver metastases: modern USA experience. J Radiat Oncol Biol Phys. 2006;65(2):412–25.
21. Ho S, Lau WY, Leung TWT, Johnson PJ. Internal radiation therapy for patients with primary or metastatic hepatic cancer. Cancer. 1998;83:1894–907.
22. Nijsen JFW, van Steenbergen MJ, Kooijman H, Talsma H, Kroon-Batenburg LMJ, van de Weert M, van Rijk PP, de Witte A, van het Schip AD, Hennink WE. Characterization of poly(L-lactic acid) microspheres loaded with holmium acetylacetonate. Biomaterials. 2001;22:3073–81.
23. Nijsen JFW, van het Schip AD, van Steenbergen MJ, Zielhuis SW, Kroon Batenburg LMJ, van de Weert M, van Rijk PP, Hennink WE. Influence of neutron irradiation on holmium acetylacetonate loaded poly(L-lactic acid) microspheres. Biomaterials. 2002;23:1831–9.
24. Vente MAD, Nijsen JFW, de Wit TC, Seppenwoolde JH, Krijger GC, Seevinck PR, Huisman A, Zonnenberg BA, van den Ingh TSGAM, van het Schip AD. Clinical effects of transcatheter hepatic arterial embolization with holmium-166 poly(L-lactic acid) microspheres in healthy pigs. Eur J Nucl Med Mol Imaging. 2008;35:1259–71.
25. Vente MAD, de Wit TC, van den Bosch MAAJ, Bult W, Seevinck PR, Zonnenberg BA, de Jong HWAM, Krijger GC, Bakker CJG, van het Schip AD, Nijsen JFW. Holmium-166 poly(L-lactic acid) microsphere radioembolization of the liver: technical aspects studied in a large animal model. Eur Radiol. 2010;20:862–9.
26. Vente MAD, Zonnenberg BA, Nijsen JFW. Microspheres for radioembolization of liver malignancies. Expert Rev Med Devices. 2010;7(5):581–3.
27. Smits MLJ, Nijsen JFW, Van Den Bosch MAAJ, Lam MGEH, Vente MAD, Huijbregts JE, Van Het Schip AD, Elschot M, Bult W, de Jong HWAM, Meulenhoff PCW, Zonnenberg BA. Holmium-166 radioembolization for the treatment of patients with liver metastases: design of the phase I HEPAR trial. J Exp Clin Cancer Res. 2010;29:70.
28. Bult W, Varkevisser R, Soulimani F, Seevinck PR, de Leeuw H, Bakker CJG, Luijten PR, van het Schip AD, Hennink WE, Nijsen JFW. Holmium nanoparticles: preparation and in vitro characterization of a new device for radioablation of solid malignancies. Pharm Res. 2010;27:2205–12.
29. Day DE, Day TE. Radiotherapy glasses. In: Hench LL, Wilson J, editors. Introduction to bioceramics, vol. 1. Singapore: World Scientific; 1993. p. 305–18.
30. Nijsen JFW, van het Schip AD, Hennink WE, Rook DW, van Rijk PP, de Klerk JMH. Advances in nuclear oncology: microspheres for internal radionuclide therapy of liver tumours. Curr Med Chem. 2002;1:73–80.
31. Cacaina D, Ylänen H, Hupa M, Simon S. Study of yttrium containing bioactive glasses behavior in simulated body fluid. J Mater Sci: Mater Med. 2006;17(8):709–16.
32. Cacaina D, Ylänen H, Simon S, Hupa M. The behaviour of selected yttrium containing bioactive glass microspheres in simulated body environments. J Mater Sci: Mater Med. 2007;19(3):1225–33.
33. Häfeli UO, Roberts WK, Pauer GJ, Kraeft SK, Macklis RM. Stability of biodegradable radioactive rhenium (Re-186 and Re-188) microspheres after neutron-activation. Appl Radiat Isot. 2001;54:869–79.
34. Conzone S, Brown RF, Day DE, Ehrhardt GJ. In vitro and in vivo dissolution behavior of a dysprosium lithium borate glass designed for the radiation synovectomy treatment of rheumatoid arthritis. J Biomed Mater Res. 2002;60:260–8.
35. Kennedy AS, Nutting C, Coldwell D, Gaiser J, Drachenberg C. Pathologic response and microdosimetry of ^{90}Y microspheres in man: review of four explanted whole livers. Int J Radiat Oncol Biol Phys. 2004;60(5):1552–63.
36. Wickremesekera JK, Chen W, Cannan RJ, Stubbs RS. Serum proinflammatory cytokine response in patients with advance liver tumors following selective internal radiation therapy (SIRT) with ^{90}Yttrium microspheres. Int J Radiat Oncol Biol Phys. 2001;49(4):1015–21.
37. Viitala R, Jokinen M, Tuusa S, Rosenholm JB, Jalonen H. Adjustably bioresorbable sol–gel derived SiO_2 matrices for release of large biologically active molecules. J Sol–Gel Sci Technol. 2005;36:147–56.
38. Peltola T, Jokinen M, Rahiala H, Levanen E, Rosenholm JB, Kangasniemi I, Yli-Urpo A. Calcium phosphate formation on porous sol–gel-derived SiO_2 and $CaO–P_2O_5–SiO_2$ substrates in vitro. J Biomed Mater Res. 1999;44:12–21.
39. Eighmy TT, Kinner AE, Shaw EL, Eusden JD Jr, Francis CA. Hydroxlapatite (Ca5(PO4)3OH) characterized by XPS: An environmentally important secondary mineral. Surf Sci Spectra. 1999;6:193–201.
40. Prado da Silva MH, Soares GA, Elias CN, Lima JHC, Schechtman H, Gibson IR, Best SM. Surface analysis of titanium dental implants with different topographies. Mater Res. 2000;3:61–7.
41. Lang WC, Padalia D, Watson LM, Fabian DJ, Norris PR. Multiplet structure in X-ray photoelectron spectra of rare earth elements and their surface oxides. Faraday Discuss. Chem. Soc. 1975;60:37–43.
42. Khattak GD, Mekki A, Wenger LE. Local structure and redox state of copper in tellurite glasses. J Non-Cryst Solids. 2004;337:174–81.
43. Simon V, Todea M, Takács AF, Neumann M, Simon S. XPS study on silica–bismuthate glasses and glass ceramics. Solid State Commun. 2007;141:42–7.
44. Zotov N, Keppler H. The influence of water on the structure of hydrous sodium tetrasilicate glasses. Am Mineral. 1998;83:823–34.
45. Massiot D, Fayon F, Capron M, King I, Le Calve S, Alonso B, Durand JO, Bujoli B, Gan Z, Hoatson G. Modelling one- and two-dimensional solid-state NMR spectra. Magn Res Chem. 2002;40:70.
46. Drake KO, Carta D, Skipper LJ, Sowrey FE, Newport RJ, Smith ME. A multinuclear solid state NMR study of the sol–gel formation of amorphous $Nb_2O_5–SiO_2$ materials. Solid State Nucl Magn Reson. 2005;27:28–36.
47. Coelho C, Babonneau F, Azais T, Bonhomme-Coury L, Maquet J, Laurent G, Bonhomme C. Chemical bonding in silicophosphate gels: contribution of dipolar and J-derived solid state NMR techniques. Sol–Gel Sci Technnol. 2006;40:181–9.